

Sea Surface Microwave Scattering at Extreme Grazing Angle: Numerical Investigation of the Doppler Shift

David Miret, Gabriel Soriano, Frédéric Nouguier, Philippe Forget, Marc Saillard, and Charles-Antoine Guérin

Abstract—We present a numerical investigation of horizontally polarized microwave scattering from 1-D sea surfaces at extreme grazing angles. Rigorous electromagnetic calculations are performed with a specific integral formalism dedicated to grazing angles. Sample sea surfaces are simulated using a classical Pierson–Moskowitz elevation spectrum together with weakly nonlinear hydrodynamic models, namely, the Creamer solution, the “choppy wave model,” and a recent improved version thereof. For this, the electromagnetic integral formalism is extended to surfaces with irregular sampling. For the different nonlinear surface models and assuming no large-scale current, we evidence a dramatic increase, followed by a saturation of the mean Doppler shift in the last few grazing degrees, with a limiting value depending quasi-linearly on the significant wave height. Our numerical investigations confirm that breaking events are not necessary to produce fast scatterers but tend to show that they are necessary to reproduce the elevated level of backscattered power. The results of this study also support the hypothesis that the blow-up of the mean Doppler shift at grazing angle is associated to an electromagnetic sharp edge effect on the large surface crests rather than geometrical shadowing of the troughs.

Index Terms—Doppler effect, method of moments, sea surface.

I. INTRODUCTION

MICROWAVE scattering from the sea surface at low grazing angles (LGAs) has important applications in ocean wave and current monitoring (e.g., [1]–[3]) or target detection (e.g., [4] and [5]). However, its simulation and understanding is still a challenging process. It has been known for a long time that the backscattered signal from the sea at grazing incidence possesses some particular features which are not visible at moderate incidences, namely, the occurrence of pronounced spikes

in the time series and the presence of “fast scatterers,” which is faster than Bragg wave, in the Doppler spectrum (e.g., [6]–[8]), especially in horizontal polarization. Even though there have been a certain number of attempts to elucidate the apparition of fast scatterers (e.g., [7], [9], and [10]), there is still no well-acknowledged theory to explain the non-Bragg mechanisms at grazing incidences. The usually invoked responsible phenomena are breaking waves, facet specular reflection by long waves, multiple-path and multibounce scattering, wedge diffraction by bound waves, and shadowing effects. However, it is still not clear whether all of these contributions are simultaneous or should be used alternatively, if at all. It is classically acknowledged that shadowing of the troughs diminishes the contribution of negative long wave orbital velocities, therefore enhancing the mean Doppler shift [7]. This is consistent with a recent numerical study [11] which identifies geometrical shadowing as one important factor in the increase of the Doppler shift. However, a recent experimental study [12] supports the converse hypothesis that geometrical shadowing has negligible contribution to LGA microwave scattering. Another controversy pertains to the actual role of breaking which is known to be related to the production of fast scatterer but not its unique origin (e.g., see discussions in [7] and [13]). The present numerical study confirms that nonbreaking hydrodynamical models can also account for very large Doppler shifts at LGA and shows that geometrical shadowing is not a relevant mechanism in this context.

In the last decade, significant progresses have been made in numerical and physical modeling of the microwave Doppler spectra. It has become clear that a rigorous electromagnetic approach [14]–[19], combined with nonlinear hydrodynamic models [20]–[22], is necessary to reproduce, at least qualitatively, the observed phenomena. In the reference paper [23] and its follow-up [24], a systematic numerical computation of Doppler spectra under different wind conditions has been conducted using a rigorous electromagnetic method and the weakly nonlinear Creamer model. As many others, this study was restricted to 1-D surfaces (2-D problem), the computational burden being otherwise prohibitive. The authors could simulate the sea echo from small to grazing incidences (0° – 85°) but did not address the last few degrees of grazing angles where the aforementioned phenomena are even more drastic. This is because the classical method of moments (MoM) based on a tapered illumination beam [25] requires the sampling of increasingly large surfaces as the incidence angle approaches 90° .

Manuscript received July 24, 2013; revised October 16, 2013 and December 21, 2013; accepted January 29, 2014. Date of publication March 17, 2014. This work was supported by the DCNS and the ANR Project No. ANR-09-BLAN-0232-01 SIMODE.

D. Miret is with Direction des Constructions Navales (DCNS), 83000 Toulon, France, with the Mediterranean Institute of Oceanography (MIO), UM 110, Université de Toulon, CNRS/INSU, IRD, 83957 La Garde, France, and also with the MIO, UM 110, Aix-Marseille Université, CNRS/INSU, IRD, 13288 Marseille, France.

G. Soriano is with Institut Fresnel, UMR 7249, Aix Marseille Université, CNRS, Centrale Marseille, 13013 Marseille, France.

F. Nouguier, P. Forget, M. Saillard, and C.-A. Guérin are with the Mediterranean Institute of Oceanography (MIO), UM 110, Université de Toulon, CNRS/INSU, IRD, 83957 La Garde, France, and also with MIO, UM 110, Aix-Marseille Université, CNRS/INSU, IRD, 13288 Marseille, France.

Digital Object Identifier 10.1109/TGRS.2014.2307893

The calculation of the scattered field at extreme grazing angles (e.g., 85° – 90°) requires a dedicated model [26], in which the sample surfaces are not prohibitively large. Owing to this adapted scattering model, we revisit the classical experiment [23] of microwave Doppler calculations from the sea surface at extreme grazing angles in the horizontal polarization case. We combine electromagnetic rigorous computations with several modern weakly nonlinear sea surface models. Note that we will not consider fully nonlinear hydrodynamic models such as those by West *et al.* [27] and Dommermuth *et al.* [28]. Even though these models have been shown [20], [22] to introduce additional effects which are not seen with weakly nonlinear models (such as increased Doppler spectral broadening and reverse travelling waves), their utilization in the context of microwave scattering by evolving surfaces raises numerical and conceptual issues which are not solved yet (particularly blow-up of high-frequency components and nonstationarity of the power spectrum). We will therefore rely only on appropriate weakly nonlinear models, namely, the Creamer representation as well as a recent Lagrangian model, the so-called choppy wave model (CWM) [29] and its recent improvement [30]. The different hydrodynamical models are reviewed in Section II. The Lagrangian models, based on perturbation expansion of the position of water particles, provide an irregular sampling of the sea surface. Since the MoM is devised for evenly sampled surfaces, this requires an adaptation of the formalism to the choppy case (Section III). The Doppler spectrum is then numerically investigated under different incidence angles and for different wind speeds using the standard Pierson–Moskowitz spectrum (Section IV). In view of the computational constraints, we focused the study on the L-band rather than the more conventional X-band. Our main observation is the blow-up, followed by a saturation, of the mean Doppler shift at LGA, with a limiting value increasing quasi-linearly with significant wave height. In the light of some numerical experiments (Section V) and experimental observations from the literature (Section VI), we discuss the possible interpretation of this phenomenon. The first clear outcome is a confirmation of the already known fact that the occurrence of breaking is not necessary to produce fast scatterers at LGA, which can be obtained with nonbreaking surface models. The second conclusion pertains to the controversy on the role of geometrical shadowing: Our observations support the hypothesis that geometrical shadowing has actually negligible impact on the enhancement of the Doppler shift at LGA, which is rather due to an edge effect at the surface crests. A third consequence of our comparisons is the compliancy of the nonbreaking models to the level of the observed Doppler shift in real conditions but not to the level of NRCS. This seems to indicate that fast scatterers are not a good proxy for sea spikes as it is sometimes claimed. At last, we investigate numerically the limiting value of the Doppler shift as the incidence angle approaches 90° and consider its evolution as a function of the sea state. A linear dependence with the significant wave height is unveiled for a wind speed smaller than 7 m/s and needs to be confirmed at larger wind speeds. It should be noted at some point that the results of this study pertain to nonrange resolved Doppler spectra, which amounts to having the illumination source at infinity. In the case of range-resolved Doppler spectra,

the observed phenomena are qualitatively different as has been shown recently [31]. In particular, there is no pronounced dependence of the mean Doppler shift on polarization or incidence, and single scattering theories are found sufficient. The elucidation of this change of nature between range-resolved and nonrange resolved Doppler spectra deserves further analysis which goes beyond the scope of this paper.

II. OCEAN SURFACE GENERATION

In the following, we chose an orthonormal system of vector $(\hat{x}, \hat{y}, \hat{z})$ and associated coordinates (x, y, z) in which the (\hat{x}, \hat{y}) plane is the mean water plane and \hat{z} is the upward directed vertical axis.

A. Linear Surfaces

In the classical linear theory, the wind-driven sea surface is written as a summation of free harmonics. Their random amplitudes are governed by the wavenumber spectrum $\Gamma(\mathbf{k})$, a function of the wave vector $\mathbf{k} = (k_x, k_y)$ which depends on sea state. Sea waves are assumed to evolve in time according to a linear dispersion relation $\omega(k)$, with $k = |\mathbf{k}|$. The field of elevations at a given time $\eta_t(\mathbf{r}) = \eta_t(x, y)$ is written as

$$\eta_t(\mathbf{r}) = \text{Re} \int A_t(\mathbf{k}) e^{i\mathbf{k}\cdot\mathbf{r}} d\mathbf{k} \quad (\text{II.1})$$

where the Fourier amplitudes are perfectly decorrelated

$$\langle A_t(\mathbf{k}) A_t^*(\mathbf{k}') \rangle = 2\Gamma(\mathbf{k}) \delta(\mathbf{k} - \mathbf{k}'). \quad (\text{II.2})$$

Asterisk denotes complex conjugate, while brackets stand for statistical average. The integral (II.1) can be numerically evaluated with efficiency through a 2-D inverse fast Fourier transform (FFT). The generation of one linear surface with $N = N_x N_y$ sampling points is thus of order $O(N \log N)$. Note that, in a given direction, sea waves propagating forward and backward generally have different amplitudes. This shows that the wavenumber spectrum $\Gamma(\mathbf{k})$ is not a true power spectrum, with centrosymmetry property. Most theoretical studies for 1-D surfaces make the canonical choice that all waves propagate in the same direction, which results in the choice of a one-sided spectrum (i.e., $\Gamma(k) = 0$ if $k < 0$).

B. Creamer Model

A popular method in the simulation of weakly nonlinear sea surface is the so-called Hamiltonian formalism [32] in its recent formulation by Creamer *et al.* [33]. The so-called Creamer model relies on a nonlinear transformation of the linear surface involving its Riesz transform (Hilbert transform in 1-D)

$$\mathbf{D}_t(\mathbf{r}) = \text{Re} \int \mathbf{i} \frac{\mathbf{k}}{k} A_t(\mathbf{k}) e^{i\mathbf{k}\cdot\mathbf{r}} d\mathbf{k}. \quad (\text{II.3})$$

The nonlinear surface $\tilde{\eta}_t$ writes as the real part of a Fourier transform (II.1) of the modified spectral amplitudes

$$\tilde{A}_t(\mathbf{k}) = \int \frac{\exp(-i\mathbf{k} \cdot \mathbf{D}_t(\mathbf{r})) - 1}{k} e^{-i\mathbf{k}\cdot\mathbf{r}} d\mathbf{r}. \quad (\text{II.4})$$

Note, however, that the form of the Fourier amplitude (II.4) precludes the use of FFT at this step and increases the numerical cost of the Creamer model to $O(N^2)$.

C. CWM

Recently, a versatile and numerically efficient weakly nonlinear model has been reintroduced [29], after the pioneering work of Pierson [34]. It was termed CWM in view of the choppy aspect of the waves it produces. It is obtained through a first-order Lagrangian expansion of particle coordinates around their rest position and produces an additional horizontal displacement with respect to a reference linear surface. It has, in common with the Creamer model, to rely on a Riesz transform, but in contradistinction to the former model, it is obtained through a shift of the horizontal (instead of vertical) coordinate. Given a linear surface η_t and its Riesz transform \mathbf{D}_t , the CWM surface $\tilde{\eta}$ is implicitly defined by

$$\tilde{\eta}_t(\mathbf{r} + \mathbf{D}_t(\mathbf{r})) = \eta_t(\mathbf{r}). \quad (\text{II.5})$$

The CWM surface is, by construction, sampled on an irregular grid as the points $\mathbf{r} + \mathbf{D}_t(\mathbf{r})$ constitute an irregular mesh of the plane. However, the pair of functions η_t , \mathbf{D}_t , hence the parametric surface $\tilde{\eta}_t$, can be efficiently generated by FFT with a cost $O(N \log N)$. This makes the method very appealing especially for 2-D surfaces. This numerical efficiency makes it possible to proceed to the calculation of 2-D Doppler spectra on nonlinear surfaces, a task which is almost dissuasive with the Creamer model. Note that the successive derivatives of the choppy surface (i.e., slopes and curvatures) can also be implicitly obtained from their linear counterparts by differentiating the relation (II.5). The geometrical transformation operated by the CWM induces a modification of the original prescribed spectrum, a process which is referred to as “dressing.” An appropriate generation of CWM would require a preliminary step of “undressing” the reference spectrum, a procedure which is discussed in [29] and [35]. The dressing of the spectrum results in a small increase of the high-frequency components of the wavenumber spectrum but is not expected to impact significantly the shape of the normalized Doppler spectrum. Therefore, we discarded this aspect in the present study.

D. Choppy 2 Wave Model

The CWM is obtained through a first-order expansion in wave steepness of Lagrangian coordinates. The monochromatic solution of the linearized equations is the well-known Gerstner waves from which the CWM has been derived. When expressed in Eulerian coordinates, it leads to weakly nonlinear wave profile. For narrow spectra, it was shown to be consistent with the classical second-order perturbation expansion [36]. However, for broader spectra, it is not fully consistent with the latter expansion and actually “miss” the contribution of some second-order terms. An improvement of the CWM was recently performed [30] by pushing the expansion at second-order in Lagrangian coordinates, a model termed the “choppy 2 wave model,” abbreviated as C2WM. It consists in adding an extra horizontal (x_2) as well as vertical (z_2) displacement to the usual CWM. This model was shown to be fully consistent with the second-order Eulerian expansion with an extended domain of validity with respect to the latter. It shows interesting nonlinear features of surface waves leading, for instance, to front-back asymmetries of wave profile and horseshoe patterns.

When expressing the Lagrangian solution back in the Eulerian framework, it can be noted [30] that only the second-order vertical (and not the horizontal) displacement of water particle contributes to the second-order Eulerian solution. In our notations and in a continuous form, this quantity writes

$$z_2(x, t) = \text{Re} \int_{-\infty}^{\infty} \int_{k' > k} \frac{A_t(k) A_t^*(k')}{g} \omega^2(k) e^{i(k-k')x} dk dk'. \quad (\text{II.6})$$

Furthermore, the horizontal displacement x_2 of water particles includes the well-known “mean Stokes drift.” As derived by Pierson, the Stokes velocity \bar{U} writes in a continuous form

$$\bar{U} = \int_{-\infty}^{\infty} \|A_t(k)\|^2 k \omega(k) dk. \quad (\text{II.7})$$

Even if this expression is in principle of second-order in the Lagrangian expansion, it results in a constant horizontal advection of the free surface which cannot be discarded with respect to the first-order contribution. It induces a secular term in the horizontal shift, which grows linearly with time and contributes to the Doppler effect. The Doppler shift resulting from this advection simply writes

$$\Delta f_{\text{Stokes}} = \frac{2\bar{U}}{\lambda_{\text{EM}}} \sin(\theta_0) \quad (\text{II.8})$$

where θ_0 is the incidence angle of the impinging electromagnetic wave. To summarize, the C2WM model which we use in the numerical simulations is obtained by adding to the CWM surface the vertical displacement z_2 defined previously and the extra Doppler shift Δf_{Stokes} arising from the mean Stokes drift.

III. MoM FOR “CHOPPY” SURFACES

The MoM [37] is a numerical technique to compute rigorous solutions of the wave scattering problem based on boundary integral equations. Since [38], it has been extensively applied to radio wave scattering from the sea surface. In its usual formulation, it involves a regular sampling of the rough surface [17], [39], [40] and can thus be used for linear as well as Creamer surfaces for which the elevation can be explicitly defined at every sampling point. For choppy surfaces, however, the sampling points are prescribed at unevenly spaced location on the horizontal axis, and the MoM requires an adaptation to such irregular sampling. The most obvious way to proceed is a mere reinterpolation of the choppy surfaces onto a regular grid. However, numerical experiments have shown that this solution must be avoided since reinterpolation introduces artificial high-frequency components which have a strong impact on the Doppler spectrum.

For simplicity and to reduce the computational burden, we restrict our study to 1-D surfaces. This corresponds to a surface being invariant along one direction, e.g., the \hat{y} direction, with an elevation $z = \eta(x)$. With the radio waves propagating much faster than water waves, the surface can be frozen at any given time t from a scattering point of view [14]. Time dependence of

the surface height and horizontal displacement $D(x)$ are thus neglected in the derivations of this section.

We consider the canonical scattering problem in which the electric field is horizontally polarized along the direction of invariance, i.e., $\mathbf{E} = E(x, z)\hat{\mathbf{y}}$. In this configuration, the scattering problem reduces from vector to scalar, as only one component of the field needs to be found. An implicit time dependence $e^{-i\omega_e t}$ at the radar frequency ω_e is assumed. The surface is further assumed to be perfectly conducting, which is a good approximation for the strongly conductive sea surface in the microwave regime under horizontal polarization.

The classical MoM formalism based on an illumination by a tapered incident beam cannot address the grazing configuration because of the limited size of the surface. This limitation can be overcome by resorting to another formalism where the surface is considered as a local deformation of an infinite plane. A specific boundary integral theory has been developed (see [41] for more details) to compute the field scattered from this finite rough patch. We develop hereafter the specific MoM formalism for choppy surfaces. To simplify the notations, we will drop the explicit time dependence of elevations ($\eta_t \rightarrow \eta$) whenever a frozen surface is considered.

An incident plane wave $E^i(x, z) = e^{i\mathbf{K}_0 \cdot \mathbf{R}} = e^{i(k_0 x - q_0 z)}$ is impinging downward on the rough interface $z = \eta(x)$ which separates air and sea water. We denote $K_0 = \omega_e/c = 2\pi/\lambda$ as the electromagnetic wavenumber, and we decompose the wave vector \mathbf{K}_0 into horizontal and vertical components ($\mathbf{K}_0 = k_0\hat{\mathbf{x}} - q_0\hat{\mathbf{z}}$). The latter is related to the incidence angle θ_0 by $k_0 = K_0 \sin \theta_0$ and $q_0 = K_0 \cos \theta_0$. Since the surface is considered as a perturbation of the infinite plane, it is natural to introduce the “mirror field” reflected by the latter, namely, $E^r(x, z) = -e^{i(k_0 x + q_0 z)}$. The total field is therefore written as the sum $E = E^i + E^r + E^d$, where E^d is the contribution of roughness only. The boundary condition at the surface (null field) implies on a CWM surface (Section II-C)

$$\begin{aligned} -E^d(x + D), \eta) &= E^i(x + D, \eta) + E^r(x + D, \eta) \\ &=: U(x) \end{aligned} \quad (\text{III.9})$$

where the x dependence is implicit in the variables η and D . We assume here and thereafter that the change of variables $x \rightarrow x + D(x)$ is univocal, which is true under the hypothesis of limited derivative of the horizontal displacement ($|D'(x)| < 1$), which is valid under the hypothesis of small slopes. The scattering problem is thus reduced to the determination of the electric surface current $\hat{\mathbf{J}}\hat{\mathbf{y}}$ which matches the discontinuity of the tangential magnetic field at the surface. Its amplitude J is proportional to the normal derivative of the electric field at the surface, i.e.,

$$\begin{aligned} J(x) &= \left(1 + \left(\frac{\eta'}{1 + D'}\right)^2\right)^{-1/2} \frac{\mathbf{i}}{\omega_e \mu_0} \\ &\quad \times \left(\frac{\partial E}{\partial z}(x + D, \eta) - \frac{\eta'}{1 + D'} \frac{\partial E}{\partial x}(x + D, \eta)\right) \end{aligned}$$

where μ_0 is the magnetic permeability of vacuum. The surface current is decomposed analogously to the electric field, i.e.,

$J = J^i + J^r + J^d$ with obvious notations. It is convenient to introduce the function

$$\begin{aligned} V(x) &= -\mathbf{i}\omega_e \mu_0 \left(1 + \left(\frac{\eta'}{1 + D'}\right)^2\right)^{1/2} J^d(x) \\ &= \frac{\partial E^d}{\partial z}(x + D, \eta) - \frac{\eta'}{1 + D'} \frac{\partial E^d}{\partial x}(x + D, \eta) \end{aligned} \quad (\text{III.10})$$

which is the unknown to be solved numerically. This leads to the following modified electric field integral equation (EFIE; [41], [42])

$$\begin{aligned} \frac{\mathbf{i}}{4} \int H_0^+(K_0 R) V(1 + D') dx' \\ = \frac{1}{2} U(x) + \frac{\mathbf{i}K_0}{4} \int \left(\Delta\eta - \frac{\eta'(x)}{1 + D'(x)}(\Delta x + \Delta D)\right) \\ \times \frac{H_1^+(K_0 R)}{R} U(1 + D') dx' \end{aligned} \quad (\text{III.11})$$

where the dependence to integration variable x' is implicit in the integrands and H_0^+ and H_1^+ are the zero- and first-order Hankel functions of the first kind. With a difference of abscissa $\Delta x + \Delta D = x - x' + D(x) - D(x')$ and a difference of elevations $\Delta\eta = \eta(x) - \eta(x')$, the interaction distance [42] between two points is $R = \sqrt{(\Delta x + \Delta D)^2 + (\Delta\eta)^2}$. Note that the vanishing of the function $U(x)$ outside a finite patch is necessary for the numerical solving of the integral (III.11).

The only functions involved in these equations are the elevations $\eta(x)$ of the linear surface, the horizontal displacement $D(x)$, and their spatial derivatives, all of which can be efficiently computed by FFT on a regular grid. Hence, the numerical implementation of the MoM for choppy surfaces reduces to a form similar to the case of evenly spaced surfaces, with different matrices, however.

The EFIE (III.11) is sampled onto a regular grid $x_i = (i - N/2)\delta x$, $i = 1, \dots, N$, and recasts in the form of a linear system $\overline{\overline{A}}\overline{\overline{X}} = \overline{\overline{B}}\overline{\overline{C}}$, where the vectors $\overline{\overline{X}}$, $\overline{\overline{C}}$ constitute the sample values of the functions V , U , respectively, and $\overline{\overline{A}}$ and $\overline{\overline{B}}$ are two full matrices with complex coefficients

$$\begin{aligned} A_{ii} &= \frac{\mathbf{i}\delta x (1 + D'_i)}{4} \left(1 + \mathbf{i}\frac{2}{\pi} \ln\left(\frac{\gamma K_0}{4e} \delta x (1 + D'_i)\right)\right) \\ A_{i \neq j} &= \frac{\mathbf{i}}{4} H_0^+(K_0 R_{ij}) (1 + D'_j) \delta x \\ B_{ii} &= \frac{1}{2} - \frac{\delta x}{4\pi} \left(\frac{\eta''_i (1 + D'_i) - \eta'_i D''_i}{(1 + D'_i)^2 + (\eta'_i)^2}\right) \\ B_{i \neq j} &= \frac{\mathbf{i}K_0 \delta x}{4R_{ij}} H_1^+(K_0 R_{ij}) \\ &\quad \times \left[\Delta\eta_{ij} - \frac{\eta'_i}{1 + D'_i}(\Delta x_{ij} + \Delta D_{ij})\right] (1 + D'_j). \end{aligned} \quad (\text{III.12})$$

Here, the subscript “ i ” denotes the evaluation of a function at a point x_i ($D_i = D(x_i)$, etc.), the subscript “ ij ” denotes the two-point difference of a function at x_i and x_j ($\Delta\eta_{ij} = \eta_i - \eta_j$, etc.), and $R_{ij} = \sqrt{(\Delta x_{ij} + \Delta D_{ij})^2 + \Delta\eta_{ij}^2}$. In view of the integrable singularity of the EFIE around $r = 0$, diagonal

terms have received specific processing following the technique developed in [42, p. 158]. Term A_{ii} involves the exponential Euler–Mascheroni constant $\gamma \simeq 1.7811$. The sampled values of $J^d(x)$ and $J(x)$ are obtained after numerical solving of the linear system. The far scattered field in direction θ_s is then obtained through the numerical evaluation (on a regular grid) of the following integral:

$$S(\theta_s) = \frac{1}{4\pi} \int \left\{ V + \mathbf{i}K_0 U \left[\sin \theta_s \frac{\eta'}{1 + D'} - \cos \theta_s \right] \right\} e^{-\mathbf{i}K_0((x+D) \sin \theta_s + \eta \cos \theta_s)} (1 + D') dx. \quad (\text{III.13})$$

The aforementioned procedure applies to CWM surfaces. As to the C2WM, it consists in a correction of elevations (not abscissa) and therefore does not require an additional change of variable. The case of linear surfaces (Section II-A) can be obtained by simply setting values to zero D and its derivatives in the aforementioned formulas.

IV. DOPPLER SPECTRA AT GRAZING ANGLES

A series of numerical computations with the MoM has been performed to evaluate the field scattered from the time-evolving sea surface at LGA. The LU decomposition technique is used to solve the linear systems in the MoM. For each test case, the linear and the three weakly nonlinear surface models (Creamer, CWM, and C2WM) have been considered. As it is classically acknowledged, the required spatial sampling rate at the surface is a fraction of the electromagnetic wavelength, while the sampling interval must be at least as large at the peak wavelength. Hence, the number of unknown grows dramatically with frequency band and wind speed. For this reason, the numerical experiments have been performed in L-band ($\lambda_{EM} = 23$ cm) at small to moderate wind speeds (from 3 to 7 m/s). In order to make meaningful comparisons with earlier studies [23], we use the conventional one-sided Pierson–Moskowitz spectrum

$$\Gamma(k) = \begin{cases} \frac{\alpha}{2k^3} \exp \left\{ -\frac{\beta g^2}{k^2 U^4} \right\}, & k > 0 \\ 0, & k \leq 0 \end{cases} \quad (\text{IV.14})$$

where U is the wind speed at 19.5 m, $g = 9.81 \text{ m} \cdot \text{s}^{-2}$ is the gravity constant, and $\alpha = 8.10 \times 10^{-3}$ and $\beta = 0.74$ are dimensionless constants. In all presented simulations, the sampling rate is $\delta x_1 = \lambda_{EM}/10 = 2.3$ cm. Time-evolving samples of the sea surface have been generated according to the different models using the gravity–capillarity wave dispersion relation $\omega(k) = \sqrt{gk(1 + k^2/k_m^2)}$, where $k_m \simeq 363.2$ rad/m is the gravity–capillarity peak. A number $N_t = 256$ of successive time samples at rate $\delta t = 25$ ms have been generated, and the corresponding complex scattering amplitude has been computed (assuming the sea surface to be frozen at each time step). For every time series of scattering amplitude, a sea surface Doppler spectrum is obtained by applying a Fourier transform and squaring the modulus. A statistical version of the Doppler spectra is obtained by further averaging over a certain number (here, $N_r = 96$) of realizations of the moving surface. At this point, it should be emphasized that no additional currents are present in the calculations of the Doppler shift from

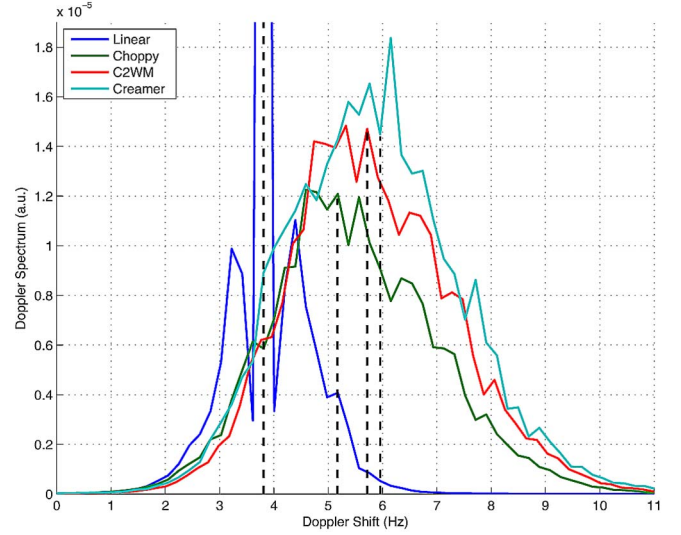


Fig. 1. L-band Doppler spectra at a wind speed of 3 m/s and an incidence angle of 89° for different surface models.

the different surface models (beside the Stokes drift in C2WM). Note that, in L-band, typical values of the current (10 cm/s) can produce a Doppler shift on the order of 1 Hz, which is on the same order of magnitude as the Doppler shift induced by wave roughness. This is a supplementary difficulty in making comparisons with experimental observations, as currents are nearly always present in the ocean. A first set of computations has been performed at 3 m/s wind speed and 89° incidence angle. The peak wavelength at this wind speed is 8.2 m, and the root mean square (rms) of elevations and slopes are, respectively, 4.8 cm and 0.137. The length of the surface samples was set to 23.6 m (thus containing at least two peak waves). Convergence tests on the surface length were performed to ensure that this is representative of an infinite surface. Fig. 1 compares the Doppler spectra $\Psi(f)$ according to the different surface models. The spectra have been normalized by the radar cross section so that $\int \Psi(f) df = 1$. The well-known features of sea Doppler spectra at LGA are recovered, namely, a significant shift and broadening of the Doppler centroid when hydrodynamic nonlinearities are taken into account. Note, however, that the various nonlinear models yield slightly different Doppler spectra. The Creamer model produces faster scatterers than the CWM but is close to the C2WM.

When waves are going in one direction only, the mean Doppler shift f_c can be defined as the first momentum of the distribution

$$f_c = \int f \Psi(f) df. \quad (\text{IV.15})$$

In the microwave regime, this quantity is known (e.g., [43]) to follow a nontrivial dependence upon the incidence angle θ_i . It is always higher than the value $f_B(\theta_i)$ predicted by the classical Bragg theory for free waves

$$f_B(\theta_i) = \frac{1}{2\pi} \sqrt{gk_B(\theta_i) \left(1 + (k_B(\theta_i)/k_m)^2 \right)} \quad (\text{IV.16})$$

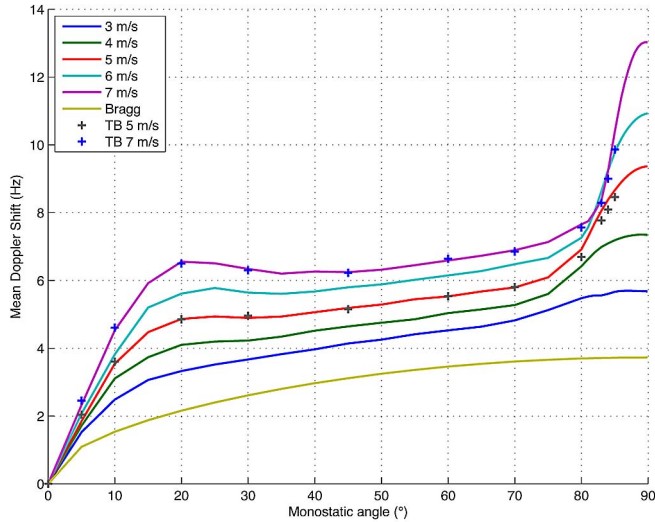


Fig. 2. Mean Doppler shift at L-band as a function of the incident angle with the Creamer model. Superimposed are the reference values of the study by Toporkov and Brown (TB) [23].

where $k_B(\theta_i) = 2k_0 \sin \theta_i$ is the so-called Bragg wavenumber. Fig. 2 shows the mean Doppler shift obtained with the Creamer model at various incidence angles and wind speeds. The angular step in this figure is 5° between 0° and 80° , 1° between 81° and 85° , and 0.5° between 85.5° and 89.5° . The final angle is 89.9° . Superimposed are the values from the reference computations of Brown and Toporkov, showing an excellent agreement in the common range of incidence angles (0° – 85°). The grazing dedicated model makes it possible to address the very last incidence angles (85 – 90) with a limited number of unknowns. This investigation at extreme angles evidences a marked behavior of the mean Doppler shift which was suggested by earlier studies, namely, a sudden and dramatic blow-up around 83° with an amplitude increasing with wind speed. A saturation occurs in the last few degrees where the mean Doppler shift reaches a plateau of variable level. Similar numerical experiments have been run with the CWM. Fig. 3 shows the sensibility to the incidence of both the Creamer and C2WM nonlinear models at 3-m/s wind speed. The same qualitative behavior is observed with smaller Doppler shift in the choppy case.

V. INTERPRETATION AND DISCUSSIONS

The salient feature of Fig. 2 is a dramatic increase of the mean Doppler shift in the last few grazing angles whenever a nonlinear surface model and a rigorous electromagnetic model are combined. This calls for a discussion on the respective contributions of nonlinear hydrodynamical mechanism and multiple-scattering effects. Nouguiet *et al.* [43] have shown that adding hydrodynamical nonlinearities in the sea surface model impacts the mean Doppler shift but also and in a more important way the Doppler spectrum width. For such derivations, they used an asymptotic electromagnetic model, namely, the weighted curvature approximation (WCA) [44], [45], which discards complex electromagnetic interactions such as multiple reflections. In that case, the discrepancies observed between linear and nonlinear surfaces are explained by modulation and advection of the short Bragg waves by longer waves. Similarly,

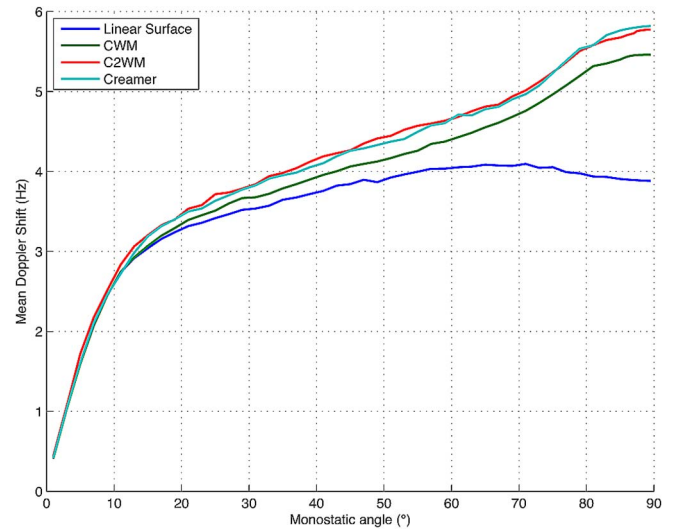


Fig. 3. Mean Doppler shift at L-band as a function of the incidence angle for different surface models and the MoM (wind speed is set to 3 m/s).

the MoM which is used in Fig. 3 illustrates the increasing influence of hydrodynamical nonlinearities with incidence angle. However, as already shown by Nouguiet *et al.* [43, Fig. 7], hydrodynamical nonlinearities are not the main factor for the enhancement of the Doppler shift, especially at high incidence angle. Indeed, the WCA model, even using the Creamer nonlinear surface model, was not capable of reproducing the dramatic increase in the last 10° of incidence. This shows that complex electromagnetic phenomena are involved in the scattering process. In the light of these numerical results, we hypothesize that the fast scatterers responsible for the large Doppler shifts are essentially due to complex electromagnetic interactions rather than scatterers with large horizontal velocities, a phenomenon which has been evoked by many authors as the consequence of breaking events. Since the weakly nonlinear hydrodynamical models which are used in this study are not capable of reproducing breaking, the simulations support the idea that the occurrence of breaking waves is not a necessary condition for the apparition of fast scatterers.

Geometrical shadowing was proposed in earlier studies (e.g., [7]) as the responsible mechanism for the blow-up of the mean Doppler shift at LGA, because it reduces the contribution of negative orbital velocities in large troughs. However, some recent observations [12] tend to show that geometrical shadowing does not actually play a role in microwave coherent backscatter from the sea surface at grazing angles. The results of our numerical simulations go along the same lines. Fig. 4 shows the evolution of the surface current with incidence angle for one frozen sample profile. The modulus is plotted, normalized by its value on the flattened edge of the sample. The corresponding profile of elevation is given at the same abscissas. Visible parts of the profile (in the sense of the geometrical optics) at 89° are highlighted with green dots. The striking feature of this figure is, first, the strong enhancement of the surface current at the crests at very large angles and, second, the stabilization of the latter at an angle of 80° (no significant changes are observed between 80° and 89°). This is very different from geometrical shadowing, which is almost nonexistent at 80° , while it is very

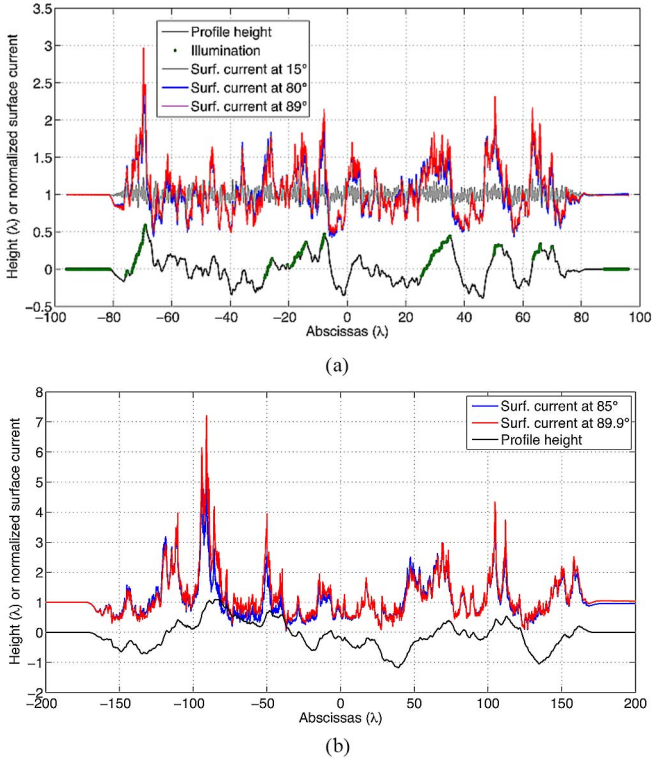


Fig. 4. Modulus of the normalized surface current at small and grazing incidence plotted together with the surface elevation profile. Wind speeds are (a) 3 m/s and (b) 7 m/s. At very large angles, the surface current is enhanced in the crests and extinguished in the troughs and does no longer evolve as the incidence angle reaches its grazing limit. The radar frequency is 1.3 GHz (L-band).

pronounced at 89°. Moreover, the enhancement of the surface current at the crests seems to be insensitive to whether the latter is in the geometrical shadow or not. Our conclusion is that the additional Doppler shift at LGA is the result of sharp edge effect at the crests rather than shadowing effect at the troughs. This is consistent with the observation that nonlinear hydrodynamic models, which exhibit sharper crests, produce a stronger positive Doppler shift than their linear counterparts. Note also that visible areas are almost identical for linear and nonlinear surfaces since weak hydrodynamical nonlinearities have little impact on the distribution of elevation (but a stronger impact on curvature).

In the absence of a full quantitative explanation of the phenomena responsible for the level of the mean Doppler shift at LGA, we have proceeded to a numerical investigation of its limiting value. Fig. 5 shows this last quantity as a function of wind speed for both the Creamer and CWM models. The extra Doppler shift with respect to this floor value is well fitted by a power-law with exponent 1.8 but different amplitude factors from one surface model to another. This quasi-quadratic dependence on wind speed suggests that a quasi-linear dependence on significant wave height could be found. Fig. 6 shows the evolution of the limiting mean Doppler shift as a function of the significant wave height (i.e., four times the rms elevation), evidencing a good match with this linear trend. The constant value predicted by the Bragg theory is given for reference. However, one should be cautious in extrapolating the results to higher wind speeds and sea states.

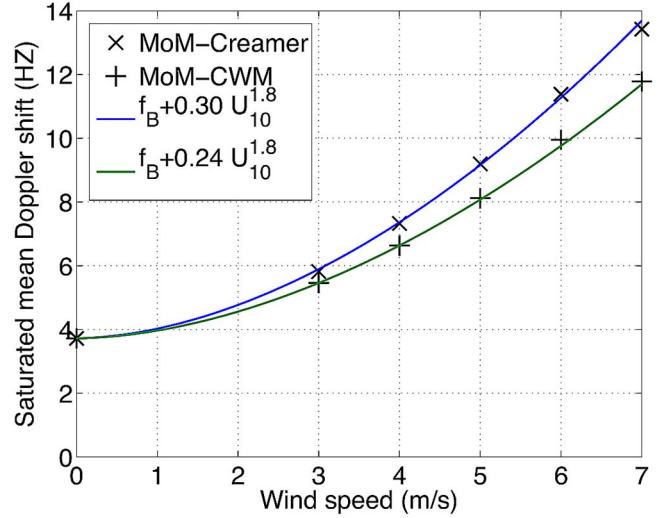


Fig. 5. Saturated mean Doppler shift at L-band as a function of wind speed for different incidence angles and hydrodynamical models.

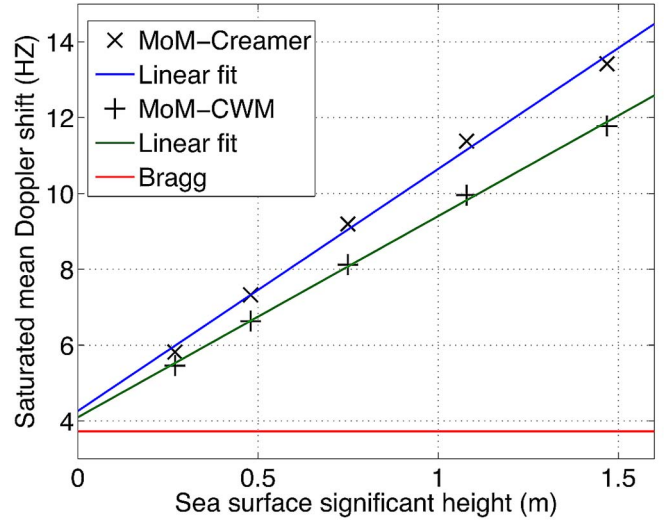


Fig. 6. Saturated mean Doppler shift at L-band as a function of significant wave height for different incidence angles and hydrodynamical models.

VI. QUALITATIVE COMPARISONS WITH EXPERIMENTAL OBSERVATIONS

The strong simplifying assumptions which underlie the theoretical model (1-D surfaces, stationary statistics, absence of current, and absence of breaking waves) make any attempt of experimental validation questionable. However, the model can be useful in unveiling the physical mechanisms at the origin of the Doppler shift, and its qualitative predictions can be analyzed in the light of experimental observations. A certain number of experiments with coherent radars illuminating the sea surface at LGA can be found in the literature, most of them operating in X-band (e.g., [6], [9], [12], [13], and [46]–[48]) and more rarely in L-band [8] and Ku-band [49]. A systematic conclusion of the aforementioned studies is the elevated level of NRCS return in HH polarization as compared to standard composite Bragg theory, the spiky nature of the backscattered power, and the occurrence of fast scatterers in the Doppler spectra. All of these

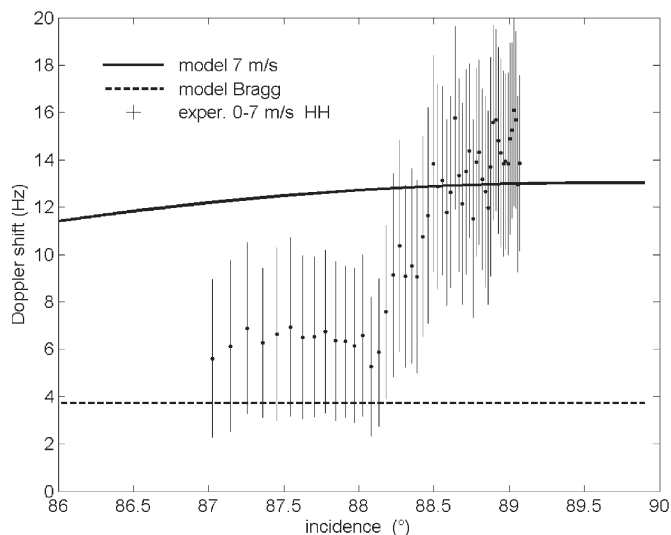


Fig. 7. L-band measurements of the Doppler shift at grazing angles (HH polarization). The different ranges of the radar cells have been converted into an angle of incidence. Dots represent the mean values of the Doppler shift, and vertical bars represent the standard deviation.

phenomena are attributed or at least correlated to the occurrence of breaking waves, a feature which could not be incorporated in the rigorous model.

Our first comparison relies on an L-band experiment conducted on the Mediterranean coast [8] using a dual polarized (VV-HH) coherent radar operating at 1.238 GHz. Grazing illumination ranged from 10° to less than 1° . Because of the complex geometry of the coast line, wave direction in conditions of well-developed stationary sea states did not always coincide with the wind direction. Therefore, one should be cautious in establishing quantitative comparisons with our simulations which address wind-driven homogeneous sea states in open sea, especially under high wind conditions. Since there is no strict correspondence between the actual experimental wind speeds and values of wind speed in the PM model, we could only make a crude overall comparison of the Doppler shifts recorded for small to moderate wind speeds. Thus, restricting the observations to wind speeds smaller than 7 m/s, we found that the range of mean measured Doppler shifts in HH is consistent with the results of the model (Fig. 7), taken here to be the 1-D MoM-Creamer model. However, a striking difference is the much faster augmentation of the mean Doppler shift with incidence as compared to the numerical results. This effect, which is also observed at higher winds, is for the moment not understood and deserves future investigation.

In addition to the Doppler shifts, it is interesting to compare, at least qualitatively, the level of absolute NRCS predicted by our simulations with experimental data. However, the backscattered power measured in the aforementioned experimental L-band study was not calibrated, and only relative NRCS could be provided. To evaluate the actual variation in incidence of the L-band NRCS, we resorted to an older but valuable data set, namely, the data cited by Nathanson *et al.* [50] in various bands, incidence, and sea state conditions. The experimental and simulated NRCSs are drawn on Fig. 8, showing the theoretical L-band NRCS at wind speeds of 5 and 7 m/s, together with the values reported from [50]. To investigate

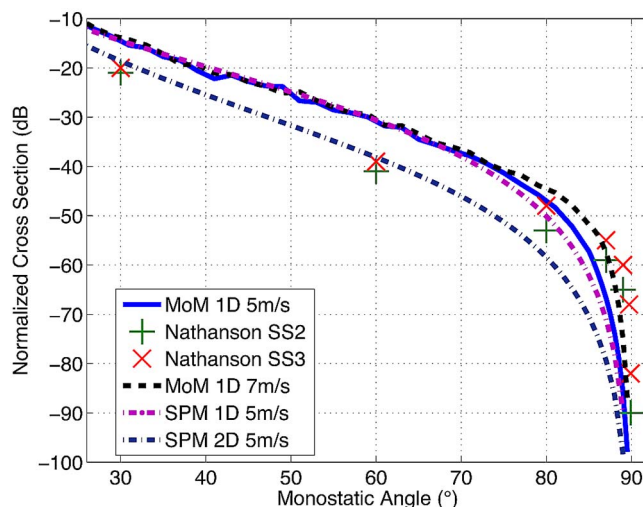


Fig. 8. L-band horizontally polarized NRCS as a function of the incidence angle. Numerical 1-D MoM simulations at 5 m/s (solid line) and 7 m/s (dashed line) wind speeds, 1-D and 2-D SPM models at 5 m/s (dashed-dotted line), and Nathanson data [50] for sea states 2 and 3 (symbols).

the effect of dimensionality on the present comparisons, the simulated NRCS has been calculated for both 1-D and 2-D surfaces using a Pierson–Moskowitz spectrum. At these wind speeds, the required number of sampling points for 2-D surfaces made the MoM prohibitive, and we used a classical small perturbation model (SPM) instead. Note that the latter is remarkably accurate over the whole range of incidence, as can be seen for 1-D surfaces where MoM could actually be run. The model comparison shows that the 1-D NRCS is about 8–10 dB higher than its 2-D counterpart at large and grazing angles. Any comparison between experimental values and 1-D simulated NRCS should account for this dimensional shift, so that the 1-D MoM NRCS should be decreased by about 10 dB when confronted to the experimental results. With this offset, we observe on Fig. 8 that the reported experimental values are already larger by 10 dB as compared to the MoM at 87° , with increasing difference (about 20–30 dB) as the grazing angle is decreased. This confirms the already known fact that any EM scattering model based on a mere surface description is unable to capture the complex hydrodynamical mechanisms, such as breaking, which are at the origin of elevated backscatter at grazing angles. Note that the occurrence of breaking crests is not bound to the presence of a strong wind field, as it can also be enhanced, for instance, by opposite-wave travelling current or variations of bathymetry.

A first partial conclusion based on L-band data is that the model is consistent with the level of the observed Doppler shift but not the level of the NRCS in the absence of breaking. This would suggest that fast scatterers are not a reliable indicator of sea spikes which are defined as very strong returns in the time series of backscattered power.

Another crude evaluation of our results can be made on the basis of some X-band data reported in the literature. In order to investigate the specific role of breaking at LGA, field data [9] were acquired in the ocean in wind conditions from 7 to 15 m/s. The backscattering cross sections and mean Doppler velocities were analyzed separately on breaking and nonbreaking

populations (a breaking event being characterized by a polarization ratio VV/HH greater than 1). Reference [9, Table 2] shows that both the average Doppler velocity and average cross section are stronger for the breaking population, this effect being more pronounced in HH polarization and at extreme grazing angles. Since the mean velocity is proportional to the mean Doppler shift, one can compare its evolution as a function of the grazing angle with our numerical simulations. The strongest wind case in the present numerical study (7 m/s) shows an increase of the mean Doppler shift from roughly 10 to 13 Hz between 5° and 1° of grazing angles (Fig. 2). An augmentation of the Doppler velocity in the same proportion (from 1.76 to 2.11 m/s) is consistently observed on the nonbreaking population but not on the breaking population for which it is almost constant (from 2.41 to 2.48 m/s). As to the mean cross section, it is diminished from about 6 and 3 dB between 5° and 1° of grazing angle for the breaking and nonbreaking populations, respectively. This confirms the conclusion drawn in L-band that the numerical simulations reproduce correctly the observed features of the Doppler shift at grazing angles in the absence of breaking, if not the absolute level of NRCS.

VII. CONCLUSION

In this paper, we have used a rigorous electromagnetic formalism dedicated to LGA microwave scattering from 1-D rough surfaces. We have investigated in the horizontal polarization case the Doppler shift arising from time-evolving sea surfaces according to different modern weakly nonlinear models. The mean Doppler shift increases slowly with the incidence at moderate angle and blows up at grazing angles where it reaches a saturation value much higher than that predicted by the classical Bragg theory. We have discussed the various phenomena involved in the production of the large Doppler shift and concluded that both complex electromagnetic and hydrodynamical interactions, but dominantly the former, are responsible for the fast increase observed at LGA. Several conclusions have been drawn from this study. First, our results support the idea that breaking events, which are not included in the hydrodynamical models under consideration, are not necessary to reproduce fast scatterers but seem necessary to reproduce the level of NRCS, a hypothesis which plays in favor of an uncoupling of sea spikes and fast scatterers. A second important outcome is that geometrical shadowing is not the dominant mechanism at the origin of these large Doppler shifts, which we rather attribute to sharp edge effect at the crests. Third, we have investigated numerically the limiting value of the mean Doppler shift at extreme incidence angle and unveiled a quasi-linear dependence of the latter with the sea surface significant wave height. The complete interpretation of this striking result requires further research.

REFERENCES

- [1] K. Reichert, J. C. N. Borge, and J. Dittmer, "WaMoS II: An operational wave monitoring system," in *Ocean Wave Measurement and Analysis (1997)*. Washington, DC, USA: ASCE, 1997, pp. 370–381.
- [2] K. Hessner, K. Reichert, and B.-L. Hutt, "Sea surface elevation maps obtained with a nautical X-band radar-examples from WaMoS II stations," in *Proc. 10th Int. Workshop Wave Hindcast. Forecast.*, 2007.
- [3] K. Reichert, K. Hessner, J. C. N. Borge, and J. Dittmer, "WaMoS II: A radar based wave and current monitoring system," in *Proc. 9th ISOPE*, Brest, France, 1999, vol. 3.
- [4] V. C. Chen, "Analysis of radar micro-Doppler with time-frequency transform," in *Proc. 10th IEEE Workshop Stat. Signal Array Process.*, 2000, pp. 463–466.
- [5] K. D. Ward, C. J. Baker, and S. Watts, "Maritime surveillance radar. I. Radar scattering from the ocean surface," *Proc. Inst. Elect. Eng. F—Radar Signal Process.*, vol. 137, no. 2, pp. 51–62, Apr. 1990.
- [6] P. H. Y. Lee, J. D. Barter, K. L. Beach, C. L. Hindman, B. M. Lake, H. Rungaldier, J. C. Shelton, A. B. Williams, R. Yee, and H. C. Yuen, "X band microwave backscattering from ocean waves," *J. Geophys. Res., Oceans*, vol. 100, no. C2, pp. 2591–2611, Feb. 1995.
- [7] P. H. Y. Lee, J. D. Barter, K. L. Beach, B. M. Lake, H. Rungaldier, H. R. Thompson, L. Wang, and R. Yee, "What are the mechanisms for non-Bragg scattering from water wave surfaces?" *Radio Sci.*, vol. 34, no. 1, pp. 123–138, Jan./Feb. 1999.
- [8] P. Forget, M. Saillard, and P. Broche, "Observations of the sea surface by coherent L band radar at low grazing angles in a nearshore environment," *J. Geophys. Res., Oceans*, vol. 111, no. C09015, Sep. 2006.
- [9] P. A. Hwang, M. A. Sletten, and J. V. Toporkov, "Breaking wave contribution to low grazing angle radar backscatter from the ocean surface," *J. Geophys. Res., Oceans*, vol. 113, no. C09017, p. C09017, Sep. 2008.
- [10] W. J. Plant and G. Farquharson, "Origins of features in wave number-frequency spectra of space-time images of the ocean," *J. Geophys. Res., Oceans*, vol. 117, no. C06015, Jun. 2012.
- [11] Y. Wang, Y. Zhang, M. He, and C. Zhao, "Doppler spectra of microwave scattering fields from nonlinear oceanic surface at moderate- and low-grazing angles," *IEEE Trans. Geosci. Remote Sens.*, vol. 50, no. 4, pp. 1104–1116, Apr. 2012.
- [12] W. J. Plant and G. Farquharson, "Wave shadowing and modulation of microwave backscatter from the ocean," *J. Geophys. Res., Oceans*, vol. 117, no. C08010, Aug. 2012.
- [13] Y. Liu, S. J. Frasier, and R. E. McIntosh, "Measurement and classification of low-grazing-angle radar sea spikes," *IEEE Trans. Antennas Propag.*, vol. 46, no. 1, pp. 27–40, Jan. 1998.
- [14] C. L. Rino, T. L. Crystal, A. K. Koide, H. D. Ngo, and H. Guthard, "Numerical simulation of backscatter from linear and nonlinear ocean surface realizations," *Radio Sci.*, vol. 26, pp. 51–71, Jan./Feb. 1991.
- [15] D. A. Kapp and G. Brown, "A new numerical method for rough surface scattering calculations," *IEEE Trans. Antennas Propag.*, vol. 44, pp. 711–721, 1996.
- [16] D. Holliday, L. L. DeRaad, and G. J. St-Cyr, "Forward-backward method for scattering from imperfect conductors," *IEEE Trans. Antennas Propag.*, vol. 46, pp. 101–108, 1998.
- [17] J. T. Johnson, "A numerical study of low-grazing-angle backscatter from ocean-like impedance surfaces with the canonical grid method," *IEEE Trans. Antennas Propag.*, vol. 46, no. 5, pp. 114–120, May 1998.
- [18] C. L. Rino and H. D. Ngo, "Numerical simulation of low-grazing-angle ocean microwave backscatter and its relation to sea spikes," *IEEE Trans. Antennas Propag.*, vol. 46, no. 1, pp. 133–141, Jan. 1998.
- [19] J. V. Toporkov and G. S. Brown, "Numerical study of the extended Kirchhoff approach and the lower order small slope approximation for scattering from ocean-like surfaces: Doppler analysis," *IEEE Trans. Antennas Propag.*, vol. 50, no. 4, pp. 417–425, Apr. 2002.
- [20] J. T. Johnson, J. V. Toporkov, and G. S. Brown, "A numerical study of backscattering from time-evolving sea surfaces: Comparison of hydrodynamic models," *IEEE Trans. Geosci. Remote Sens.*, vol. 39, no. 11, pp. 2411–2420, Nov. 2001.
- [21] H. Kim and J. T. Johnson, "Radar image study of simulated breaking waves," *IEEE Trans. Geosci. Remote Sens.*, vol. 40, no. 10, pp. 2143–2150, Oct. 2002.
- [22] A. R. Hayslip, J. T. Johnson, and G. R. Baker, "Further numerical studies of backscattering from time evolving non-linear sea surfaces," *IEEE Trans. Geosci. Remote Sens.*, vol. 41, no. 10, pp. 2287–2293, Oct. 2003.
- [23] J. V. Toporkov and G. S. Brown, "Numerical simulations of scattering from time-varying, randomly rough surfaces," *IEEE Trans. Geosci. Remote Sens.*, vol. 38, no. 4, pp. 1616–1624, Jul. 2000.
- [24] J. V. Toporkov and M. A. Sletten, "Statistical properties of low-grazing range-resolved sea surface backscatter generated through two-dimensional direct numerical simulations," *IEEE Trans. Geosci. Remote Sens.*, vol. 45, no. 5, pp. 1181–1197, May 2007.
- [25] E. I. Thorsos, "The validity of the Kirchhoff approximation for rough surface scattering using a Gaussian roughness spectrum," *J. Acoust. Soc. Amer.*, vol. 83, no. 1, pp. 78–92, 1988.
- [26] M. Saillard and A. Sentenac, "Rigorous solutions for electromagnetic scattering from rough surfaces," *Waves Random Media*, vol. 11, no. 3, pp. R103–R137, 2001.

- [27] B. J. West, K. A. Brueckner, R. S. Janda, D. M. Milder, and R. L. Milton, "A new numerical method for surface hydrodynamics," *J. Geophys. Res., Oceans*, vol. 92, no. C11, pp. 11 803–11 811, Oct. 1987.
- [28] D. G. Dommermuth and D. K. P. Yue, "A high-order spectral method for the study of nonlinear gravity waves," *J. Fluid Mech.*, vol. 184, no. 1, pp. 267–288, 1987.
- [29] F. Nouguier, C.-A. Guérin, and B. Chapron, "Choppy wave model for nonlinear gravity waves," *J. Geophys. Res., Oceans*, vol. 114, pp. C09012-1–C09012-16, Sep. 2009.
- [30] F. Nouguier and C.-A. Guérin, "Second order Lagrangian description of random tridimensional gravity waves. The "choppy 2 wave model"," *J. Fluid Mech.*, to be published.
- [31] C.-S. Chae and J. T. Johnson, "A study of sea surface range-resolved Doppler spectra using numerically simulated low-grazing-angle backscatter data," *IEEE Trans. Geosci. Remote Sens.*, vol. 47, no. 6, pp. 3452–3460, Jun. 2013.
- [32] V. E. Zakharov, "Stability of periodic waves of finite amplitude on the surface of a deep fluid," *J. Appl. Mech. Tech. Phys.*, vol. 9, no. 2, pp. 190–194, Mar./Apr. 1968.
- [33] D. B. Creamer, F. Henyey, R. Schult, and J. Wright, "Improved linear representation of ocean surface waves," *J. Fluid Mech.*, vol. 205, pp. 135–161, 1989.
- [34] W. J. Pierson, *Models of Random Seas Based on the Lagrangian Equations of Motion*. New York, NY, USA: Dept. of Meteorology, College of Eng., New York Univ., 1961.
- [35] F. Nouguier, C.-A. Guérin, and B. Chapron, "Scattering from nonlinear gravity waves: The choppy wave model," *IEEE Trans. Geosci. Remote Sens.*, vol. 48, no. 12, pp. 4184–4192, Dec. 2010.
- [36] M. S. Longuet-Higgins, "The effect of non-linearities on statistical distributions in the theory of sea waves," *J. Fluid Mech.*, vol. 17, no. 3, pp. 459–480, 1963.
- [37] R. F. Harrington, *Field Computation by Moment Methods*. New York, NY, USA: Macmillan, 1968.
- [38] R. R. Lentz, "A numerical study of electromagnetic scattering from ocean-like surface," *Radio Sci.*, vol. 9, no. 12, pp. 1139–1146, 1974.
- [39] L. Tsang, "Monte Carlo simulations of large-scale composite random rough-surface scattering based on the banded-matrix iterative approach," *J. Opt. Soc. Amer. A*, vol. 11, no. 2, pp. 691–696, Feb. 1994.
- [40] J. T. Johnson, "On the canonical grid method for two-dimensional scattering problems," *IEEE Trans. Antennas Propag.*, vol. 46, no. 3, pp. 297–302, Mar. 1998.
- [41] G. Soriano, P. Spiga, and M. Saillard, "Low-grazing angles scattering of electromagnetic waves from one-dimensional natural surfaces: Rigorous and approximate theories," *Comptes Rendus Phys.*, vol. 11, no. 1, pp. 77–86, Jan. 2010.
- [42] L. Tsang, J. A. Kong, K. H. Ding, and C. O. Ao, *Scattering of Electromagnetic Waves: Numerical Simulations*. New York, NY, USA: Wiley-Interscience, 2001, ser. Wiley series in remote sensing.
- [43] F. Nouguier, C.-A. Guérin, and G. Soriano, "Analytical techniques for the Doppler signature of sea surfaces in the microwave regime-II: Nonlinear surfaces," *IEEE Trans. Geosci. Remote Sens.*, vol. 49, no. 12, pp. 4920–4927, Dec. 2011.
- [44] C.-A. Guérin, G. Soriano, and T. Elfouhaily, "Weighted curvature approximation: Numerical tests for 2D dielectric surfaces," *Waves Random Media*, vol. 14, no. 3, pp. 349–363, 2004.
- [45] C.-A. Guérin, G. Soriano, and B. Chapron, "The weighted curvature approximation in scattering from sea surfaces," *Waves Random Complex Media*, vol. 20, no. 3, pp. 364–384, 2010.
- [46] D. S. W. Kwoh and B. M. Lake, "A deterministic, coherent, and dual-polarized laboratory study of microwave backscattering from water waves, Part I: Short gravity waves without wind," *IEEE J. Ocean. Eng.*, vol. 9, no. 5, pp. 291–308, Dec. 1984.
- [47] D. S. W. Kwoh, B. M. Lake, and H. Rungaldier, "Microwave scattering from internal wave modulated surface waves: A shipboard real aperture coherent radar study in the Georgia strait experiment," *J. Geophys. Res., Oceans*, vol. 93, no. C10, pp. 12235–12248, Oct. 1988.
- [48] S. J. Frasier, Y. Liu, and R. E. McIntosh, "Space-time properties of radar sea spikes and their relation to wind and wave conditions," *J. Geophys. Res., Oceans*, vol. 103, no. C9, pp. 18 745–18 757, Aug. 1998.
- [49] A. D. Rozenberg, D. C. Quigley, and W. Kendall Melville, "Laboratory study of polarized microwave scattering by surface waves at grazing incidence: The influence of long waves," *IEEE Trans. Geosci. Remote Sens.*, vol. 34, no. 6, pp. 1331–1342, Nov. 1996.
- [50] F. E. Nathanson, J. P. Reilly, and M. N. Cohen, *Radar Design Principles: Signal Processing and the Environment*. Raleigh, NC, USA: SciTech Publ., 1999.

David Miret was born in Suresnes, France, in 1987. He received the M.S. degree in physics and engineering from the Ecole Centrale Paris, Châtenay-Malabry Cedex, France, in 2007. He is currently working toward the Ph.D. degree at Direction des Constructions Navales (DCNS), Toulon, France.

He is a member of the DCNS Electromagnetic Compatibility Team collaborating with the Mediterranean Institute of Oceanography, Toulon, and the Fresnel Institute, Marseille, France.



Gabriel Soriano was born in Paris, France, in 1972. He received the M.S. and Ph.D. degrees in physics from Paul Cezanne University, Marseille, France, in 1996 and 2000, respectively.

He is currently an Associate Professor with Aix-Marseille University, Provence, France. He is a member of the ElectroMagnetical and Optical Remote Sensing and CONCEPT research teams of the Fresnel Institute, Marseille. He works on electromagnetic wave scattering from rough surfaces and associated numerical methods, as well as on effects of disordered media on light polarization.

Frédéric Nouguier received the "Agrégation" and M.S. degrees in applied physics from the Ecole Normale Supérieure de Cachan, Cachan, France, in 2005 and 2006, respectively, the M.S. degree in physical methods for remote sensing from the University of Paris-Diderot, Paris, France, in 2006, and the Ph.D. degree in physics from the University of Marseille, Marseille, France, in 2009.

From 2009 to 2010, he was a Postdoctoral Fellow with the French Research Institute for Exploitation of the Sea (Ifremer), Brest, France. In 2011 he was working on synergical studies of optical and synthetic aperture radar sensors products in mesoscale and submesoscale ocean dynamics interpretation at Ifremer, Brest as a European Space Agency Postdoctoral Fellow. He is currently an Associate Professor at the Mediterranean Institute of Oceanography, Toulon, France and is working on nonlinear interactions of gravity waves.

Philippe Forget received the B. Eng. degree from the Ecole Nationale Supérieure des Techniques Avancées, Paris, France, in 1974, the "Thèse de 3e Cycle" in oceanography from Paris VI University, Paris, France, in 1979, and the "Thèse de Doctorat d'Etat" in oceanography from Sud Toulon-Var University, Toulon, France, in 1983.

He is currently the Director of Research at the Centre National de la Recherche Scientifiques (CNRS) at the Mediterranean Institute of Oceanography (CNRS/IRD/Aix-Marseille and University of Toulon). He has worked in various fields of coastal oceanography (surface waves, coastal dynamics, internal waves, ocean-atmosphere interactions), electromagnetism (scattering by the sea surface, radio wave propagation), ocean optics and remote sensing (HF/VHF radars, synthetic aperture radar and other microwave techniques, optical sensors). He has been involved in several mission projects of Centre National d'Etudes Spatiales (CNES, Toulouse) and has conducted several oceanographic and remote sensing (airborne) field campaigns.



Marc Saillard was born in Marseille, France, in 1961. He received the "Agrégation" degree in physics and the Ph.D. degree from the University of Marseille, Marseille, in 1985 and 1990, respectively.

From 1990 to 1997, he was an Assistant Researcher with the Electromagnetic Optics Laboratory, National Center for Scientific Research (CNRS). In 1997, he became a Professor with the University of Marseille, where he ran the remote sensing group of the Institut Fresnel. In 2003, he moved to the University of Toulon, Toulon, France,

as a Professor, where he joined the Remote Sensing Laboratory (LSEET). In 2011, he was elected as the President of the University of Toulon. His scientific interests lie in ocean microwave sensing, modelization and analysis of the sea surface radar signature, and imaging through random media.

Charles-Antoine Guérin, photograph and biography not available at the time of publication.